Applied Acoustics 200 (2022) 109050

Contents lists available at ScienceDirect

Applied Acoustics

journal homepage: www.elsevier.com/locate/apacoust

Broadband directional resonant tunneling emission enhancement via acoustic anisotropic metamaterials

Yunzhong Lei, Jiu Hui Wu *, Zhen Huang, Libo Wang, Yao Huang

School of Mechanical Engineering & State Key Laboratory for Strength and Vibration of Mechanical Structures, Xi'an Jiao Tong University, Xi'an 710049, China

ARTICLE INFO

Article history:
Received 6 July 2022
Received in revised form 28 August 2022
Accepted 25 September 2022

Keywords:
Broadband emission enhancement
Directional resonant tunneling
Acoustic anisotropic metamaterials

ABSTRACT

Broadband directional acoustic emission enhancement is essential in practical applications, such as acoustic communication and medical imaging. In this paper, an anisotropic metamaterial array of meta-unit consisting of a straight channel and four symmetrical side branch cavities is proposed, aiming to achieve broadband directional resonant tunneling acoustic emission enhancement via the coupling of the transmission peaks in the y-direction. In the range of 3335–4625 Hz, the broadband anisotropic characteristic is reflected in the opposite transmission capacities of the meta-unit and periodic array in the orthogonal directions, which is caused by the different effective impedances due to resonant tunneling. Numerical simulation shows that for the anisotropic metamaterial array with a monopole source in the center, the broadband directional acoustic emission enhancement phenomenon appears in the y-direction. The experimental results confirm that at a distance of 35 cm from the point source, the SPL gain in the y-direction is 4 dB on average, and the SPL in the x-direction is reduced by an average of 12 dB. Based on the above results, the proposed anisotropic metamaterial array is expected to show significant potential applications in the fields where broadband acoustic signals are required.

1. Introduction

Directional acoustic emission has attracted more and more interest in the past decades due to its broad application prospects, including loudspeaker designs [1], acoustic communication [2], and medical diagnostics [3]. The previous methods of realizing directivity mainly rely on the active methods to modify the acoustic source, such as phased array technology, which has the problems of many electronic components and complicated circuits. Therefore, it is necessary to develop a new and efficient passive directional acoustic emission technology. Acoustic metamaterials are man-made materials used to manipulate sound waves, which have properties that are difficult to achieve in nature, such as negative mass density [4], negative bulk modulus [5], double negative metamaterials [6], and extreme anisotropy [7]. Based on the properties, metamaterials can manipulate sound waves in the wavelength range to produce various functions. Therefore, many functional devices with unique performance applications have been developed, such as subwavelength imaging systems [8–13], acoustic waveguides [14–16], sound insulators [17–19], and sound absorbers [20–22].

Based on the emerging acoustic metamaterials, various schemes to control the directionality of the acoustic waves have been discussed [23–27]. Ke investigated the radiation of a point acoustic source placed inside a two-dimensional phononic crystal of square lattice. A highly directional sound source with large radiation enhancement can be obtained at the band-edge frequencies of the phononic crystal [25]. Acoustic metasurface [28–30], as a category of acoustic metamaterials, has the characteristics of simple and compact structure, and flexible and effective control of waves. The propagation of the acoustic waves can be flexibly controlled by adjusting the phase distribution of the acoustic field via the generalized Snell's law. Therefore, it is usually used to realize the directional emission of plane waves [31–35]. Li proposed a tunable curved metasurface composed of corrugated cells to realize the directional propagation of acoustic waves [35]. Compared with plane waves, the realization of acoustic emission directional enhancement of the monopole source is more challenging. To solve this, a sub-wavelength Mie resonance structure is proposed to achieve the radiation directionality of monopole sources [36–37] Lu designed a sub-wavelength space-coiling structure to strongly control the acoustic radiation pattern. A collimated beam at low frequencies is realized based on its inherent monopolar Mie Resonance [37]. However, the directional acoustic emission only works in a narrow specific Mie resonance frequency band, which

* Corresponding author.
E-mail address: ejhwu@xjtu.edu.cn (J.H. Wu).

https://doi.org/10.1016/j.apacoust.2022.109050
0003-682X/

seriously affects their application in practical situations. Recently, due to the flexible sound propagation control, many new acoustic devices have been designed using acoustic metamaterials with anisotropic characteristics [38–43]. Directional acoustic emission enhancement can also be realized by anisotropic acoustic metamaterials based on resonance and gradient impedance [44–45]. Qiao proposed a metamaterial consisting of a unit array composed of a square cavity and two symmetrical straight channels. The anisotropic properties of metamaterials exist in the range of 8430–9460 Hz, and based on the anisotropic properties, the wavefront-invariant enhanced directional acoustic emission is realized [44]. Jia proposed a two-way spiral-shaped metamaterial array, which exhibited almost opposite transmission properties in orthogonal directions due to impedance matching design. Finally, directional acoustic emission enhancement is realized in the range of 4.8–5.8 kHz [45]. However, how to further increase the bandwidth of directional acoustic emission enhancement is still an urgent problem to be solved.

Based on the observations above, the purpose of this paper is to realize broadband directional acoustic emission enhancement. To obtain satisfactory results, we propose an anisotropic metamaterial array of meta-unit consisting of a straight channel and four symmetrical side branch cavities. Through the studies of dispersion relations and equivalent parameters, the proposed meta-unit and periodic array have broadband anisotropic properties in the range of 3335–4625 Hz, which are validated by the near-full transmission in the y-direction and the acoustic isolation in the x-direction. The specific relationship between the transmissions and parameters of the anisotropic metamaterial is investigated thoroughly, aiming to guide the design of the broadband anisotropic metamaterial. Based on the above analysis, the broadband directional acoustic emission enhancement is achieved by placing a point sound source in the center of the anisotropic metamaterial array. The experimental results verify the simulation conclusions.

The rest of the paper is organized as follows: in Section 2, the proposed metamaterial array is introduced and the anisotropic property and mechanism are revealed through finite element calculations; in Section 3, The effect of the key parameters on the anisotropic property is investigated in detail; in Section 4, the directional acoustic emission enhancement performance of the proposed metamaterial array is verified by simulation and experiment. Finally, Section 5 gives several conclusions.

2. Structure design, anisotropic property and mechanism

In this section, the proposed metamaterial array is presented, in addition, the finite element calculation results show that it possesses anisotropic property, and the reason for the anisotropy is explained by the band diagram and the effective acoustic impedance of the meta-unit.

The schematic illustration of the periodically distributed anisotropic metamaterial array (15 × 7) is shown in Fig. 1. The meta-unit composed of a straight channel and four symmetrical side branch cavities is presented in the red dotted rectangle. The width and length of the meta-unit are a = 15 mm and b = 35 mm, the channel width is c = 3 mm, and half inner channel length is d = 5.8 mm and the outer channel length e = 3.7 mm. The width of the side branch cavity is m = 4 mm, and the wall thickness is t = 1 mm. Based on the finite element analysis software COMSOL Multiphysics, the anisotropic properties of the meta-unit and periodic array are investigated. The background air parameters are mass density $\rho = 1.21\ kg/m^3$ and sound velocity v = 343 m/s. The used material of the array is epoxy resin, with the elastic modulus, Poisson's ratio, and the density of 5.08 GPa, 0.35, and $1.21\ kg/m^3$, respectively. Besides, the frameworks of the anisotropic metamaterial are set as acoustically rigid.

First, to demonstrate the anisotropic property of the proposed metamaterial, a full-wave simulation model is established to calculate the transmission spectrum with different unit numbers (n), as shown in Fig. 2(a) and 2(c). A plane wave with an amplitude of 1 Pa is incident from the x-direction and y-direction of the metamaterial in the form of a background pressure field, respectively. The perfectly matched layers are added to both edges of the plane wave

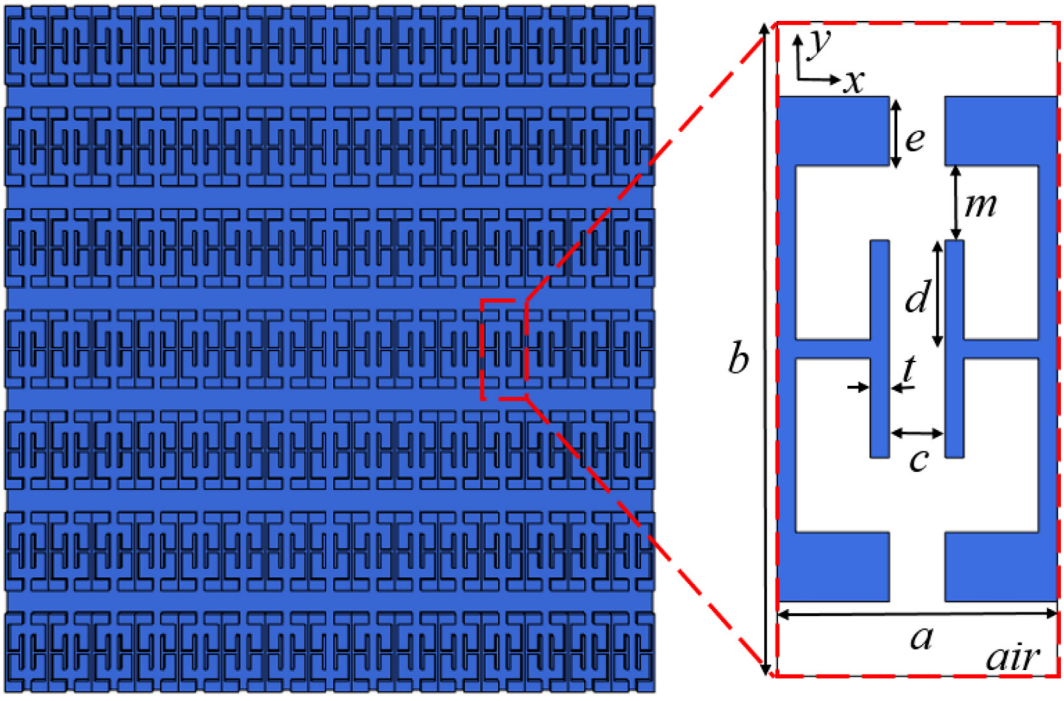

Fig. 1. Schematic of the anisotropic metamaterial array and the meta-unit composed of a straight channel and four symmetrical side branch cavities.

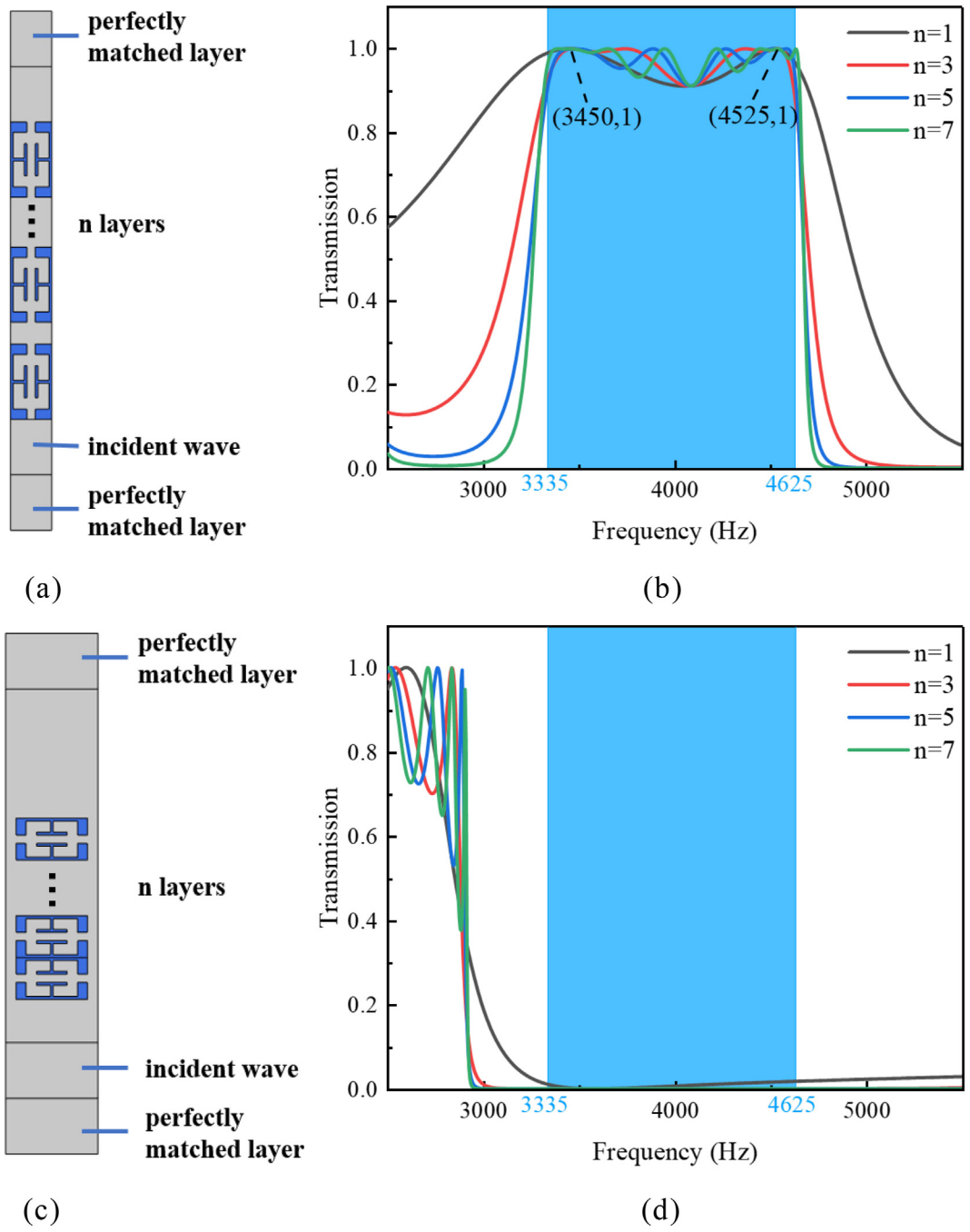

Fig. 2. The simulation model and boundary conditions for transmission spectrum in y (a) and x (c) directions. Transmission spectrum in y (b) and x (d) directions for different numbers (n) of meta-units.

incident direction to eliminate boundary reflection, and the results are shown in Fig. 2(b) and 2(d), respectively. The black line, red line, blue line, and green line represent the transmittances when n = 1, 3, 5, and 7, respectively. It is found that for different n, in the range of 3335–4625 Hz (light blue shadow region), the transmittance in the y-direction is greater than 0.9 and reaches 1 at some frequencies, while the transmittance in the x-direction is close to zero. Therefore, the meta-unit and periodic array with broadband anisotropic characteristics in the x and y directions in the range of 3335–4625 Hz are proved.

To intuitively analyze the acoustic wave propagation properties in orthogonal directions in the metamaterial array, the pressure field distributions in the free space, the x-direction, and the y-direction of the metamaterial array in the range of 3335–4625 Hz are simulated when the plane wave is incident. The simulated distributions of normalized sound pressure field at 3540 Hz are shown in Fig. 3(a)-(c). By comparing with the simulation in free space, it is obvious that in the x-direction, the sound wave can hardly pass through the metamaterial array, resulting in a large reduction in the sound pressure amplitude on the right side of the metamaterial array. However, the sound waves pass almost perfectly through the y-direction of the metamaterial array as can be seen by comparing the normalized sound pressure amplitudes on the left and right sides. Additionally, the waveform remains unchanged after passing through the array. Therefore, it is further demonstrated that the proposed metamaterial array

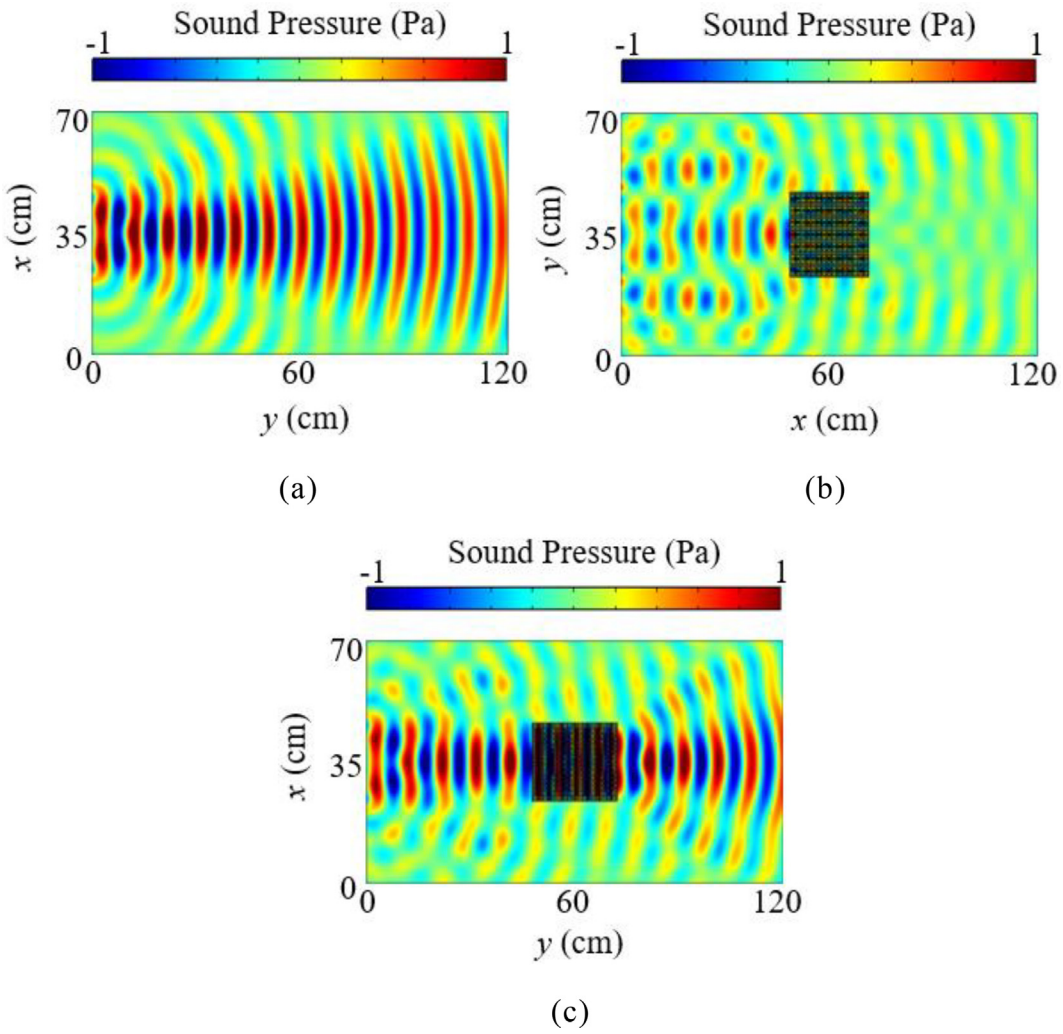

Fig. 3. The simulated distributions of the pressure fields in the free space (a), x-direction (b), and y-direction (c) of the metamaterial array at 3540 Hz when a plane wave is incident.

possesses the characteristic of broadband anisotropy, which manifests as opposite acoustic wave propagation properties in orthogonal directions.

Next, to analyze the causes of the anisotropic characteristics, Bloch's periodic boundary condition is applied at the boundary of the meta-unit, and the corresponding characteristic frequencies are calculated by the wave vector components kx and ky along the edge of the irreducible Brillouin zone. The obtained band diagram and the first Brillouin zone are presented in Fig. 4. It can be observed that the passband appears in the ΓY direction and the bandgap appears in the ΓX direction in the frequency range of 3335–4625 Hz (light blue shadow region). To reveal the mechanism of directional bandgap generation, the relative effective parameters of the meta-unit are calculated through the complex transmission and reflection coefficients based on the equivalent medium theory, which are normalized by the air parameters. Fig. 5 shows the effective impedances of the meta-unit in the x and y directions. The red and blue lines represent the effective acoustic impedances in the x and y directions, respectively, and the solid and dashed lines represent the real and imaginary parts of the impedance, respectively. In the range of 3335–4625 Hz, the real part of the impedance is close to zero in the x-direction but the imaginary part can be non-negligible. Therefore, the acoustic wave cannot pass through the meta-unit in the x-direction due to the mismatched impedance between the meta-unit and air. However, in the y-direction, the real part of the impedance is around 1.0, and the imaginary part is close to zero. In particular, the frequencies corresponding to 1.0 for the real part of the impedance are 3450 Hz and 4525 Hz, which are consistent with the frequencies corresponding to the transmission peaks when n = 1 in Fig. 2. This behavior means that the phenomenon of resonant tunneling at perfectly impedance-matched frequencies allows sound waves to propagate perfectly through the metamaterial array. Therefore, the acoustic impedances of the meta-unit and air are well matched in a wide frequency range in the y-direction due to resonant tunneling, and sound waves can pass through the meta-unit efficiently. Based on the above, it is demonstrated that the generation of the directional bandgap is caused by the different effective acoustic impedances in the x and y directions in a large range of 3335–4625 Hz. Therefore, the periodic array has broadband anisotropic characteristics, exhibiting completely different transmission characteristics between the x-direction and y-direction.

3. Effect of key parameters on broadband anisotropy characteristics

For the perspective of the results of the above analysis, the realization of broadband anisotropy strongly depends on the meta-

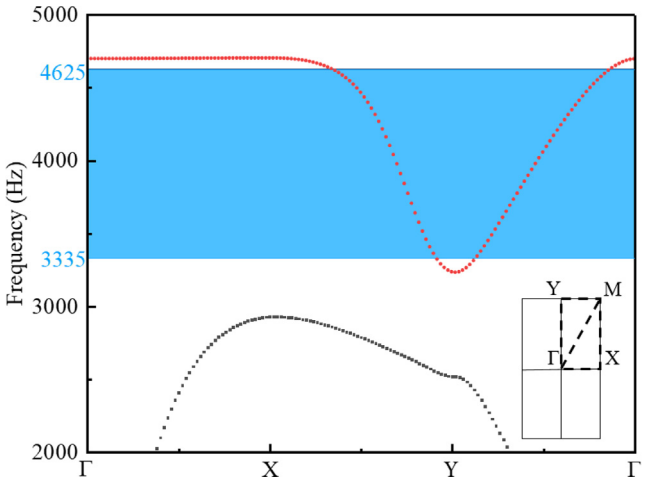

Fig. 4. The band diagram and the first Brillouin zone.

unit parameters. In this section, the dependences of the transmission on the parameters are investigated thoroughly through theoretical analysis and simulation, which aims to provide a general rule of the broadband anisotropic characteristic design.

In essence, the process of a plane wave passing through the meta-unit in the y-direction can be regarded as the propagation of a plane wave in the channel with variable cross-sections. The schematic diagram of the equivalent model is shown in Fig. 6(a). In this case, we can establish the connection of the sound waves on both sides of the variable cross-section through two boundary conditions at the section, that is, the sound pressure continuity and the volume velocity continuity. Then through the layer-by-layer recursion, the ratio of the transmitted acoustic wave and the incident acoustic wave is finally obtained, thereby obtaining the transmission coefficient.

For example, in the first variable section cross-section at y = 0:

$$p_i + p_{1r} = p_{2t} + p_{2r} \tag{1}$$

$$S_1(v_i + v_{1r}) = S_2(v_{2t} + v_{2r}) \tag{2}$$

...

In the last variable cross-section:

$$p_{6t} + p_{6r} = p_t \tag{3}$$

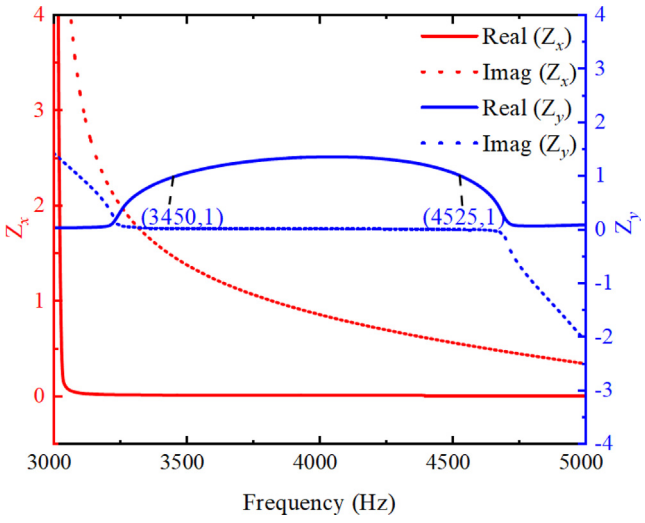

Fig. 5. The effective acoustic impedance of the meta-unit in the x and y directions.

$$S_6(v_{6t}e^{-jkl_6} + v_{6r}e^{-jkl_6}) = S_7 v_t \tag{4}$$

where, p_i and p_t are the sound pressure amplitudes of the incident and transmitted waves, respectively. The subscript numbers represent the channel, the subscript r and t represent the transmitted and reflected waves in the channel, respectively, S is the channel width and l is the channel length, $v_t = p_t/\rho_0 c_0$ and $v_r = -p_r/\rho_0 c_0$ are the particle motion velocities of the transmitted and reflected waves in the channel, respectively.

Fig. 6(b) shows the transmission spectrum of different m in the x and y directions, where the solid line and the dotted line represent the transmission in the y and x directions, respectively. The black line, red line, blue line, and green line represent the transmission when m = 3.5 mm, 4 mm, 4.5 mm, 5 mm, and other parameters remain constant, respectively. It is obvious that with the increase of m in the y-direction, the two transmission peaks both move to the lower frequencies, the first transmission peak decreases more slowly than the second, and the transmission of the corresponding frequency region in the x-direction is close to zero. So the anisotropic band moves to the lower frequency region and the bandwidth becomes smaller. This behavior can be explained from a simple perspective: in the y-direction, the meta-unit can be equivalent to a spring-mass system, where the outer and inner channels are equivalent to masses m_1 and m_2, respectively, and the side cavity is equivalent to a spring with stiffness k. When m increases, the stiffness of the system decreases so that the two resonant tunneling frequencies decrease. Fig. 6(c) shows the effect of parameter c on the transmission spectrum with other parameters remaining unchanged. It is clear that as c increases in the y-direction, both transmission peaks move to higher frequencies, and the transmission of the corresponding frequency region in the x-direction is close to zero. The reason for the phenomenon is that in the y-direction, with the increase of c, the mass of the system decreases, and from the inverse relationship between the resonance frequency and the mass, the resonance frequency increases.

Fig. 6(d)-(e) show the effects of parameters d, and e on the transmission spectrum when other parameters remain unchanged. For parameter d, with the increase of parameter d in the y-direction, both transmission peaks move to lower frequencies, and the decline speed of the first transmission peak is much smaller than that of the second transmission peak. On the contrary, for parameter e, with the increase of parameter e in the y-direction, both transmission peaks move to lower frequencies, and the decline speed of the first transmission peak is much larger than that of the second transmission peak. The transmission in the x-direction for the corresponding frequency region is close to zero. The reason for this behavior can be explained: in the y-direction, with the increase of d and e, the mass of the system increases, and from the inverse relationship between the resonance frequency and the mass, the resonance frequency decreases. Parameter d has a greater impact on the second resonant tunneling frequency than first resonant tunneling frequency, and parameter e is just the opposite, resulting in the results shown in Fig. 6(e). The observations provide a design principle to achieve low-frequency anisotropy: by increasing the width of the side branch cavity m, half inner channel length d, the outer channel length e, and decreasing the channel width c.

Fig. 6(f) shows the transmission spectrum of different e in the x and y directions when the sum of d and e is constant and other parameters remain constant, where the parameter e is chosen as 3.5 mm, 4.0 mm, 4.5 mm, 5.0 mm, and d + e = 9.5 mm. The solid line and the dotted line respectively represent the transmission in the y and x directions through the simulation. The results show that with the decrease of e in the y-direction, the first transmission peak moves to a higher frequency but the second moves to a lower

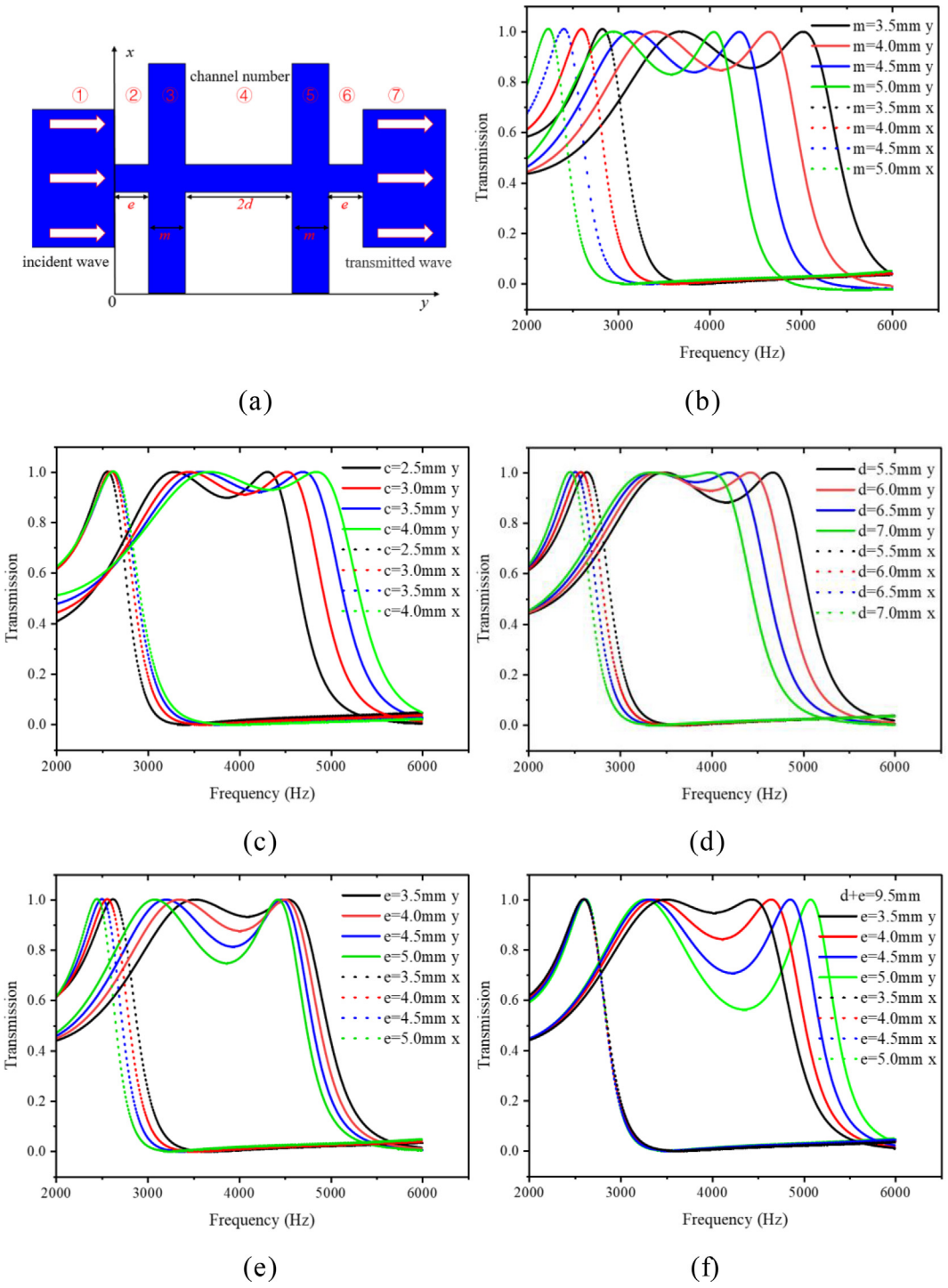

Fig. 6. The schematic diagram of the equivalent model (a). The transmission spectrum for different m (b), c (c), d (d), and e (e). The transmission spectrum for different d (f) when the sum of d and e is a constant.

frequency, and the transmission of the corresponding frequency region in the x-direction is still close to zero. From the changes of the system m_1, m_2 and k, it is inferred that the reason for the result is that with the decrease of e, m_1 decreases, m_2 increases, and k increases. Under the changing trend, the first resonance tunneling frequency increases, and the second resonance tunneling frequency decreases. This observation provides a design principle to achieve broadband anisotropic properties through the coupling of the two transmission peaks induced by resonant tunneling: by varying the inner and outer channel lengths.

4. The realization of broadband directional acoustic emission enhancement

After parameter optimization, the parameters we choose are the same as those shown in Fig. 1. To verify the proposed anisotropic metamaterial array has potential application value in broadband directional acoustic emission enhancement. We replace one meta-unit located in the center of the periodic array with a point sound source generating cylindrical wave radiation to simulate the distribution of the sound pressure field. Fig. 7(a)-7(b) show

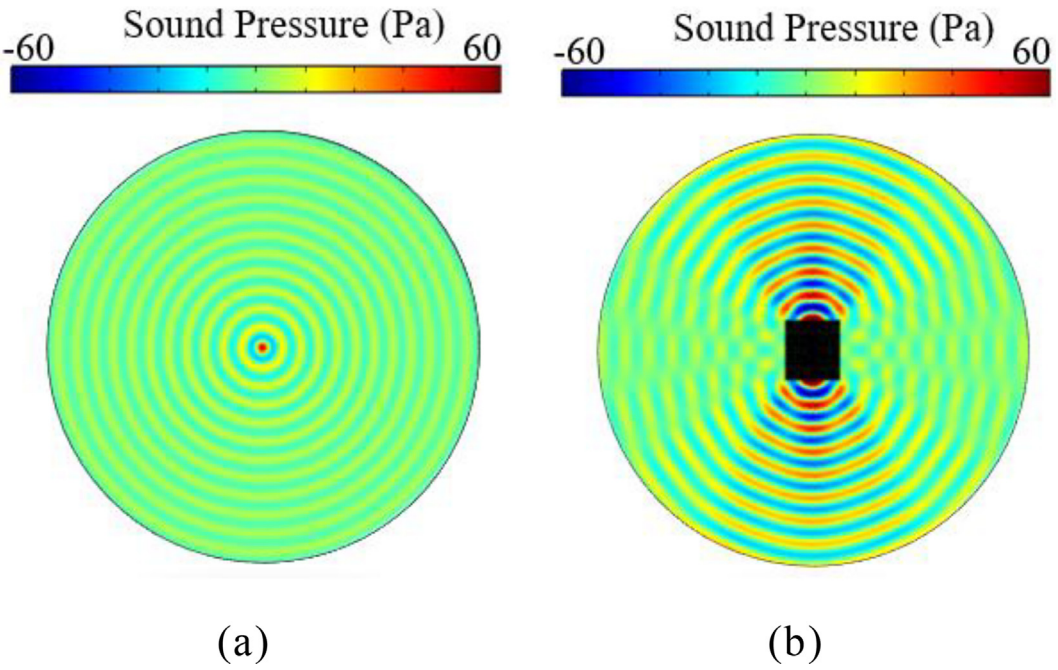

Fig. 7. The simulation of the pressure field distributions of a point sound source in free space (a) and the center of the metamaterial array (b) at 3540 Hz.

the simulated pressure field distribution in the presence of the metamaterial array and free space at 3540 Hz, respectively. It is observed that the distribution of the sound pressure field in the x and y directions of the free space is the same. However, when the anisotropic metamaterial array exists, the sound pressure amplitude in the y-direction is significantly enhanced and the output waveform remains unchanged, but the sound pressure amplitude in the x-direction is reduced. The results can be interpreted that the anisotropic metamaterial array in the range of 3335–4625 Hz in the x-direction is a forbidden band, and in the y-direction is a passband, so the propagation of sound waves in the x-direction is prohibited, and the point sound source emission is restricted to the y-direction. Therefore, the proposed metamaterial has the potential for broadband directional acoustic emission enhancement.

Finally, we further verify the performance of broadband directional acoustic emission enhancement by comparing the SPL gains at 35 cm from the point source in the orthogonal direction obtained from the experimental measurements and simulation results. The experimental setup is shown in Fig. 8(a). Through 3D printing technology, the metamaterial array with the central meta-unit removed is precisely fabricated using epoxy resin. Due to the large acoustic impedance mismatch between the air medium and epoxy resin, the 3D printed samples can satisfy the hard acoustic field boundary conditions used for the simulation. The experimental sample with a height of 12 mm is sandwiched between the two-dimensional waveguides consisting of two parallel acrylic plates. The point source is placed in the center of the experimental sample and sealed, and the two microphones are placed in the orthogonal directions to obtain sound pressure at a distance of 35 cm from the point source. The sound-absorbing cotton is placed at the edge of the waveguide to eliminate the effects of reflections due to impedance mismatch. The digitizer is used to obtain the measured sound pressure amplitude. Fig. 8(b) shows the simulated and experimentally measured SPL gains in the presence of the metamaterial array compared to free space at 35 cm from the point source in the orthogonal direction. The black and red lines represent the simulated SPL gain in the orthogonal direction without considering the thermal-viscous loss, respectively, and the

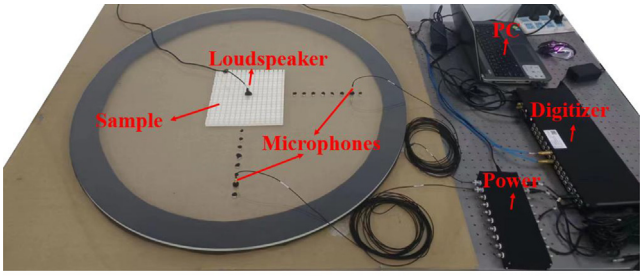

(a)

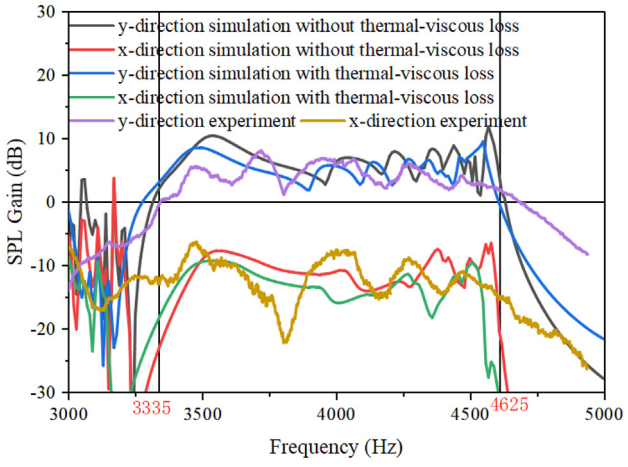

(b)

Fig. 8. (a) Photograph of the experimental setup. (b) The SPL gain in the presence of the metamaterial array measured by simulation and experiment at a distance of 35 cm from the point source in the orthogonal direction.

blue and green lines represent the SPL gain obtained by the simulation in the orthogonal direction when the thermal-viscous loss is considered. It can be seen that when the thermal-viscous loss is

present, the simulated SPL gain is lower at 3335–4625 Hz compared to the SPL gain without the thermal-viscous loss, and the peaks shift to low frequencies. By comparing the SPL gains in the y and x direction with and without thermal-viscous loss, we can find that in the range of 3335–4625 Hz, the proposed metamaterial array can achieve broadband directional acoustic emission enhancement. The purple line and the yellow line represent the SPL gain in the orthogonal direction obtained through the experiment. It is observed that the experimental and the simulation results are consistent in trend. In the range of 3335–4625 Hz, the average SPL gains in the y-direction and x-direction are 4 dB and −12 dB, respectively. This further confirms the ability of the proposed metamaterial array to possess anisotropic properties and broadband directional acoustic emission enhancement. The deviation between the experimental value and the simulation result can be attributed to the error in the printing of the sample, the failure of the two acrylic plates to be completely parallel, the gap between the sample acrylic plates, and scattered waves having a strong reverse effect on the source due to the loudspeaker being very close to the meta-unit.

5. Conclusion

In this study, an anisotropic metamaterial composed of a straight channel and four symmetrical side branch cavities is proposed. By adjusting parameters d and e, the transmission peaks in the y-direction caused by resonant tunneling are coupled, and the metamaterial array with broadband anisotropic characteristics is realized in the range of 3335–4625 Hz. Through the studies of dispersion relationships and equivalent parameters, it is demonstrated that the generation of the directional band gap is caused by the difference in the effective acoustic impedances in the x and y directions. Therefore, the proposed periodic array has broadband anisotropic properties of the prohibition of acoustic transmission in the x-direction and high-efficiency acoustic transmission in the y-direction. Based on the anisotropic characteristic, when the point sound source is placed in the center of the periodic array, the experimental results show that the metamaterial array has excellent broadband enhanced directional acoustic emission performance. In the range of 3335–4625 Hz, at a distance of 35 cm from the point source, the SPL gain in the y-direction is 4 dB on average, and the SPL in the x-direction is reduced by an average of 12 dB. The research provides new guidance for the realization of broadband directional acoustic emission enhancement and shows great potential in the fields where broadband acoustic signals are required.

CRediT authorship contribution statement

Yunzhong Lei: Conceptualization, Methodology, Software, Validation, Formal analysis, Investigation, Data curation, Writing – original draft, Writing – review & editing. **Jiu Hui Wu:** Writing – review & editing. **Zhen Huang:** Validation, Formal analysis, Investigation, Data curation. **Libo Wang:** Validation, Writing – review & editing. **Yao Huang:** Software, Validation.

Data availability

Data will be made available on request.

Declaration of Competing Interest

The authors declare that they have no known competing financial interests or personal relationships that could have appeared to influence the work reported in this paper.

Acknowledgment

This work is supported by the National Natural Science Foundation of China (Nos. 51675401).

References

[1] Shi C, Gan WS. Product directivity models for parametric loudspeakers. J Acoust Soc Am 2012;131:1938–45.
[2] Zhang Z, Tian Y, Wang Y, Gao S, Cheng Y, Liu X, et al. Directional Acoustic Antennas Based on Valley-Hall Topological Insulators. Adv Mater 2018;30:1803229.
[3] Bucci OM, Crocco L, Scapaticci R, Bellizzi G. On the Design of Phased Arrays for Medical Applications. Proc IEEE 2016;104:633–48.
[4] Liu Z, Zhang X, Mao Y, Zhu YY, Yang Z, Chan CT, et al. Locally Resonant Sonic Materials. Science 2000;289.
[5] Fang N, Xi D, Xu J, Ambati M, Srituravanich W, Sun C, et al. Ultrasonic metamaterials with negative modulus. Nat Mater 2006;5:452–6.
[6] Ding Y, Liu Z, Qiu C, Shi J. Metamaterial with simultaneously negative bulk modulus and mass density. Phys Rev Lett 2007;99:093904.
[7] Chen Y, Liu H, Reilly M, Bae H, Miao Y. Enhanced acoustic sensing through wave compression and pressure amplification in anisotropic metamaterials. Nat Commun 2014;5:5247.
[8] Zhu J, Christensen J, Jung J, Martin-Moreno L, Yin X, Fok L, et al. A holey-structured metamaterial for acoustic deep-subwavelength imaging. Nat Phys 2010;7:52–5.
[9] Jia H, Ke M, Hao R, Ye Y, Liu F, Liu Z. Subwavelength imaging by a simple planar acoustic superlens. Appl Phys Lett 2010;97.
[10] Li B, Deng K, Zhao H. Acoustic guiding and subwavelength imaging with sharp bending by sonic crystal. Appl Phys Lett 2011;99.
[11] Cheng Y, Zhou C, Wei Q, Wu D, Liu X. Acoustic subwavelength imaging of subsurface objects with acoustic resonant metalens. Appl Phys Lett 2013;103.
[12] Christensen J, García de Abajo FJ. Acoustic field enhancement and subwavelength imaging by coupling to slab waveguide modes. Appl Phys Lett 2010;97.
[13] Jia H, Lu M, Wang Q, Bao M, Li X. Subwavelength imaging through spoof surface acoustic waves on a two-dimensional structured rigid surface. Appl Phys Lett 2013;103.
[14] Lemoult F, Kaina N, Fink M, Lerosey G. Wave propagation control at the deep subwavelength scale in metamaterials. Nat Phys 2012;9:55–60.
[15] Babaee S, Overvelde JTB, Chen ER, Tournat V, Bertoldi K. Reconfigurable origami-inspired acoustic waveguides. Sci Adv 2016;2:e1601019.
[16] Park CM, Kim CH, Park HT, Lee SH. Acoustic gradient-index lens using orifice-type metamaterial unit cells. Appl Phys Lett 2016;108.
[17] Li F, Zhe C, Zhang SY, Jin D, Li XJ, Hui Z. An acoustic metamaterial composed of multi-layer membrane-coated perforated plates for low-frequency sound insulation. Appl Phys Lett 2015;106:151908.
[18] Xiao Y, Wen J, Wen X. Sound transmission loss of metamaterial-based thin plates with multiple subwavelength arrays of attached resonators. J Sound Vib 2012;331:5408–23.
[19] Fleury R, Sounas DL, Sieck CF, Haberman MR, Alu A. Sound Isolation and Giant Linear Nonreciprocity in a Compact Acoustic Circulator. Science 2014;343:516–9.
[20] Jimenez N, Huang W, Romero-Garc V, Pagneux V, Groby J-P. Ultra-thin metamaterial for perfect and quasi-omnidirectional sound absorption. Appl Phys Lett 2016;109:121902.
[21] Xu Q, Qiao J, Sun J, Zhang G, Li L. A tunable massless membrane metamaterial for perfect and low-frequency sound absorption. J Sound Vib 2021;493.
[22] Zhu XF, Lau SK, Lu Z, Jeon W. Broadband low-frequency sound absorption by periodic metamaterial resonators embedded in a porous layer. J Sound Vib 2019;461:114922.
[23] Quan L, Zhong X, Liu X, Gong X, Johnson PA. Effective impedance boundary optimization and its contribution to dipole radiation and radiation pattern control. Nat Commun 2014;5:3188.
[24] Zhou Y, Lu MH, Feng L, Ni X, Chen YF, Zhu YY, et al. Acoustic surface evanescent wave and its dominant contribution to extraordinary acoustic transmission and collimation of sound. Phys Rev Lett 2010;104:164301.
[25] Ke M, Liu Z, Pang P, Qiu C, Zhao D, Peng S, et al. Experimental demonstration of directional acoustic radiation based on two-dimensional phononic crystal band edge states. Appl Phys Lett 2007;90.
[26] Shen C, Xie Y, Sui N, Wang W, Cummer SA, Jing Y. Broadband Acoustic Hyperbolic Metamaterial. Phys Rev Lett 2015;115:254301.
[27] Jiang X, Zhang LK, Liang B, Zou XY, Cheng JC. Ultra-broadband absorption by acoustic metamaterials. Appl Phys Lett 2015;107:093506.
[28] Ma G, Yang M, Xiao S, Yang Z, Sheng P. Acoustic metasurface with hybrid resonances. Nat Mater 2014;13:873–8.
[29] Li Y, Shen C, Xie Y, Li J, Wang W, Cummer SA, et al. Tunable Asymmetric Transmission via Lossy Acoustic Metasurfaces. Phys Rev Lett 2017;119:035501.
[30] Li Y, Assouar BM. Acoustic metasurface-based perfect absorber with deep subwavelength thickness. 2016;108:063502.
[31] Chen D-C, Zhu X-F, Wei Q, Yao J, Wu D-J. Broadband tunable focusing lenses by acoustic coding metasurfaces. J Phys D Appl Phys 2020;53.

[32] Peng X, Ji J, Jing Y. Composite honeycomb metasurface panel for broadband sound absorption. J Acoust Soc Am 2018;144:EL255.
[33] Gong K, Zhou X, Ouyang H, Mo J. Continuous manipulation of acoustic wavefront using a programmable acoustic metasurface. J Phys D Appl Phys 2021;54.
[34] Fan S-W, Zhao S-D, Cao L, Zhu Y, Chen AL, Wang Y-F, et al. Reconfigurable curved metasurface for acoustic cloaking and illusion. Phys Rev B 2020;101.
[35] Li X-S, Wang Y-F, Chen AL, Wang Y-S. An arbitrarily curved acoustic metasurface for three-dimensional reflected wave-front modulation. J Phys D Appl Phys 2020;53.
[36] Cheng Y, Zhou C, Yuan BG, Wu DJ, Wei Q, Liu XJ. Ultra-sparse metasurface for high reflection of low-frequency sound based on artificial Mie resonances. Nat Mater 2015;14:1013–9.
[37] Lu GX, Ding EL, Wang YY, Peng XY, Cui J, Liu XZ, et al. Realization of acoustic wave directivity at low frequencies with a subwavelength Mie resonant structure. Appl Phys Lett 2017;110:123507.
[38] Zigoneanu L, Popa BI, Cummer SA. Three-dimensional broadband omnidirectional acoustic ground cloak. Nat Mater 2014;13:352–5.
[39] Popa BI, Zigoneanu L, Cummer SA. Experimental acoustic ground cloak in air. Phys Rev Lett 2011;106:253901.
[40] Gu Y, Cheng Y, Liu X. Acoustic planar hyperlens based on anisotropic density-near-zero metamaterials. Appl Phys Lett 2015;107.
[41] Li J, Fok L, Yin X, Bartal G, Zhang X. Experimental demonstration of an acoustic magnifying hyperlens. Nat Mater 2009;8:931–4.
[42] Gu Z-m, Xue J, Liang B, Li Y, Zou X-Y, Yin L-L, et al. Experimental realization of broadband acoustic omnidirectional absorber by homogeneous anisotropic metamaterials. J Appl Phys 2015;117.
[43] Jiang X, Liang B, Li R-q. Zou X-y, Yin L-l, Cheng J-c. Ultra-broadband absorption by acoustic metamaterials. Appl Phys Lett 2014;105.
[44] Qian J, Sun H-x. Yuan S-q, Liu X-j. Enhanced directional acoustic emission based on anisotropic metamaterials. Appl Phys Lett 2019;114.
[45] Jia X, Yan M, Hong M. Sound energy enhancement via impedance-matched anisotropic metamaterial. Mater Des 2021;197.